

**PARTICLE SIZE EFFECT ON MECHANICAL AND THERMAL  
PROPERTIES OF SiO<sub>2</sub> PARTICULATE POLYMER COMPOSITES**

by

Jae-Soon Jang

A thesis submitted to the Faculty of the University of Delaware in partial fulfillment of the requirements for the degree of Master of Science in Mechanical Engineering

Summer 2012

© 2012 Jae-Soon Jang  
All Rights Reserved

**PARTICLE SIZE EFFECT ON MECHANICAL AND THERMAL  
PROPERTIES OF SiO<sub>2</sub> PARTICULATE POLYMER COMPOSITES**

by

Jae-Soon Jang

Approved: \_\_\_\_\_  
Jonghwan Suhr, Ph.D.  
Professor in charge of thesis on behalf of the Advisory Committee

Approved: \_\_\_\_\_  
Suresh G. Advani, Ph.D.  
Chair of the Department of Mechanical Engineering

Approved: \_\_\_\_\_  
Babatunde A. Ogunnaike, Ph.D.  
Interim Dean of the College of Engineering

Approved: \_\_\_\_\_  
Charles G. Riordan, Ph.D.  
Vice Provost for Graduate and Professional Education

## ACKNOWLEDGMENTS

First of all, I would like to thank my advisor Dr. Jonghwan Suhr, for his help, encouragement, technical guidance and financial support. Secondly, I would like to thank Dr. Hyung-ick Kim, James Sargianis, Joshua Varischetti and other group members for their help with mechanical testing and research. Thirdly, I would like to thank Dr. Ronald F. Gibson for his help, insightful conversations and research. Fourthly, I would like to acknowledge the National Science Foundation for financial support. I also would like to thank the Center for Composite Materials (CCM) for kindly providing me with the DSC and autoclave facility access. I also would like to give special thanks to Dr. Bingqing Wei and Dr. Erik Thostenson for reviewing my thesis and being members of my thesis committee.

Finally, I am eternally grateful to my parents and my wife, Jungin Cho, for their encouragement, constant love and support. Most of all, I express my thanks to God for giving me life, health and faith.

*“The one who sent me is with me; he has not left me alone,  
for I always do what pleases him.” (John 8:29)*

## TABLE OF CONTENTS

LIST OF TABLES .....	vi
LIST OF FIGURES .....	vii
ABSTRACT .....	ix

### Chapter

1	INTRODUCTION .....	1
1.1	Particulate Polymer Composites.....	1
1.2	Past Studies on Particle Size Effects .....	2
1.3	Goals and Thesis Organization.....	3
2	MECHANICAL AND THERMAL PROPERTIES OF PARTICULATE POLYMER COMPOSITES .....	5
2.1	Material & Composite Fabrication .....	5
2.1.1	Material.....	5
2.1.2	Composite Fabrication.....	5
2.2	Experimental, Results & Discussion .....	10
2.2.1	Measurement of Glass Transition Temperature .....	10
2.2.2	Measurement of Coefficient of Thermal Expansion .....	11
2.2.3	Measurement of Young's Modulus .....	13
2.2.4	Measurement of Tensile Toughness .....	16
2.2.5	Measurement of Fracture Toughness .....	17
3	A PARTICLE SIZE-DEPENDENT "EFFECTIVE PARTICLE VOLUME FRACTION" .....	22
3.1	Interphase Region for Size Effect.....	22
3.2	The Concept of Effective Particle Volume Fraction .....	24
3.3	Finite Element Modeling.....	25
3.3.1	Geometry of the Model .....	26

3.3.2	Mechanical Properties and Interphase Model .....	27
3.3.3	Elements, Meshing and Boundary Conditions .....	28
3.3.4	Young's Modulus Determination .....	30
3.3.5	Interphase Region Thickness.....	30
3.4	Results & Discussion.....	31
4	CONCLUSIONS .....	33
5	FUTURE WORK .....	35
	REFERENCES .....	36

## LIST OF TABLES

<b>Table 2.1:</b> Glass transition temperature of the particulate composites at various volume fractions up to 15% of 20nm and 10 $\mu$ m SiO <sub>2</sub> particles .....	10
<b>Table 3.1:</b> Length ( $\mu$ m) of the cubic side for 10 $\mu$ m and 20nm size particles for 1% volume fraction .....	26
<b>Table 3.2:</b> Material properties of particle and matrix [1,60] .....	27
<b>Table 3.3:</b> Interphase region properties (simplified) .....	28

## LIST OF FIGURES

<b>Figure 2.1:</b> A schematic illustration of composite fabrication process .....	6
<b>Figure 2.2:</b> Sample cure condition of the 20nm and 10 $\mu$ m SiO <sub>2</sub> particulate composites .....	7
<b>Figure 2.3:</b> Results of DSC characterization of neat epoxy .....	8
<b>Figure 2.4:</b> (a) SEM images of fracture surface of 15vol % of SiO <sub>2</sub> (10 $\mu$ m) particulate composites (b) TEM images of 15vol % of SiO <sub>2</sub> (20nm) particulate composites at higher magnification .....	9
<b>Figure 2.5:</b> Experimentally determined CTE of the particulate composites at various volume fractions of 20nm and 10 $\mu$ m SiO <sub>2</sub> particles .....	12
<b>Figure 2.6:</b> Stress-strain curves of (a) the 20nm SiO <sub>2</sub> particulate composites at various volume fractions and (b) 10 $\mu$ m 20nm SiO <sub>2</sub> particulate composites at various volume fractions .....	14
<b>Figure 2.7:</b> Experimentally determined Young's modulus of the particulate composites at various volume fractions of 20nm and 10 $\mu$ m SiO <sub>2</sub> particles.....	16
<b>Figure 2.8:</b> Experimentally determined tensile toughness of the particulate composites at various volume fractions of 20nm and 10 $\mu$ m SiO <sub>2</sub> particles.....	17
<b>Figure 2.9:</b> Experimentally determined fracture toughness of the particulate composites at various volume fractions of 20nm and 10 $\mu$ m SiO <sub>2</sub> particles.....	19
<b>Figure 2.10:</b> Fracture energy of the particulate composites at various volume fractions of 20nm and 10 $\mu$ m SiO <sub>2</sub> .....	21
<b>Figure 3.1:</b> Spherical particle surrounded by interphase region.....	25
<b>Figure 3.2:</b> Simplified: the interphase region is divided into three sections to approximate the linear variation of properties across its thickness .....	28
<b>Figure 3.3:</b> Typical 3D view of the meshed 1/8 domain finite element model .....	29

<b>Figure 3.4:</b> Roller-slider boundary conditions on planes $X=0$ , $Y=0$ , and $Z=0$ and Multi-Point Constraint (MPC) on the three other faces of 1/8 domain model.....	30
<b>Figure 3.5:</b> Calculated results for FE models with and without interphase region compared with experimental values at particle volume fraction of 1 vol% .....	32
<b>Figure 3.6:</b> $\Delta R/R$ and $v_{\text{eff}}$ from FE model with interphase region at particle volume fraction of 1 vol% .....	32

## ABSTRACT

The objective of this thesis is to investigate the effect of the particle size on mechanical and thermal properties of both micro- and nano sized SiO<sub>2</sub> particulate composites over a wide range of particle volume fractions. In this study, spherically shaped 10µm and 20nm SiO<sub>2</sub> particles, and diglycidyl ether of bisphenol A (DGEBA) are used as fillers and as matrix material, respectively. While 10µm SiO<sub>2</sub> particles are dispersed in the epoxy through a direct shear mixing method, nano-composites are fabricated by using commercially available standard Nanopox F400 (nanoresins AG, Germany) with hardener (Albidur HE600) at desirable volume fractions up to 15vol%. All samples were examined for cure degree and particle dispersion quality by the use of differential scanning calorimetry (DSC) and scanning electron microscopy (SEM) or transmission electron microscopy (TEM), respectively.

The glass transition temperature of samples was identified by DSC and mechanical dynamic analysis (DMA). Using thermal mechanical analysis (TMA), the thermal stability of the samples was evaluated. This study also employs tensile and fracture testing to characterize the tensile properties including Young's modulus ( $E$ ), tensile toughness, and fracture toughness ( $K_{IC}$ ). In the test results, 20nm SiO<sub>2</sub> particulate composites show greater Young's modulus and fracture toughness than 10µm SiO<sub>2</sub> particulate composites at the same volume fraction.

Finally, a combined numerical/experimental approach is used to study the effects of the particle/matrix interphase on the Young's modulus of SiO<sub>2</sub> particulate nanocomposites having nanoparticle reinforcements of different sizes. Our experiments showed that the composite Young's modulus increases with decreasing nanoparticle diameter at the same volume fraction, but our finite element (FE) model predictions did not match the expected trends when the interphase was not accounted for. The new models include an interphase region around the nanoparticle which

results in an “effective particle volume fraction” that is larger than the actual particle volume fraction. The results from the models are compared with the experimental results and the new models are accurately fitted to the experimental results using the interphase thickness as a curve-fitting parameter. This is the first study on the use of combined numerical/experimental investigations of elastic stiffness characteristics to demonstrate the existence of a particle size-dependent “effective particle volume fraction” due to the particle/matrix interphase region in a particulate nanocomposite.

## Chapter 1

### INTRODUCTION

#### 1.1 Particulate Polymer Composites

Mechanical and thermal stability are of crucial importance in development of lightweight composite structures for aerospace, mechanical, and civil systems where extreme environments and operating temperatures are not unusual. Many researches have been studied to improve the mechanical as well as thermal stability of polymer matrix. Recently, various fillers have been widely used to improve the mechanical properties of polymer composite because filler materials can modify the physical and mechanical properties of polymer materials [1-10]. It has been shown that dramatic improvements in mechanical and thermal properties can be achieved by the incorporation of particulate fillers, such as micro or nano silicon dioxide ( $\text{SiO}_2$ ), glass, aluminum oxide ( $\text{Al}_2\text{O}_3$ ), calcium carbonate ( $\text{CaCO}_3$ ), carbon nanotube (CNT), carbon nanofiber (CNF) and so on.

Among these various fillers, glass beads or ceramic particles have been commonly used for improvement of Young's modulus, fracture toughness and thermal stability since they are isotropic, have relatively high strength and stiffness, carry a low coefficient of thermal expansion and have low cost [1, 11-16]. For example, Zhang et al. [12] reported that the  $\text{SiO}_2$  particles were able to improve the stiffness of the epoxy materials when the interparticle distance was smaller than the  $\text{SiO}_2$  particle diameter. Hsieh et al. [13] considered the Young's modulus of four different epoxy polymers containing 0, 10 and 20wt%  $\text{SiO}_2$  particle. Ma et al. [14] investigated the

effect of silica nanoparticles on the mechanical properties of two epoxy systems cured by two different curing agents. Hatta et al. [15] found that silica particles were able to reduce the CTE in the particulate composites.

## **1.2 Past Studies on Particle Size Effects**

In the previous studies, glass beads or ceramic (e.g. silica or silicon dioxide; SiO<sub>2</sub>) particles with various diameters from nano- and micron were used. From these studies, it was found that smaller size particles lead to better mechanical properties of particulate composites than larger particle reinforced composites. Smaller size particles, however, give rise to some manufacturing issues including high viscosity and uniform dispersion at high particle loading fractions [17]. In recent years, the effects of particle size on mechanical performance of particulate composites have been studied by many researchers [17-26]. For instance, Cho et al. [17] experimentally observed that both Young's modulus and tensile strength of glass beads and alumina nanoparticle reinforced composites were increased when nanoparticle size was decreased at the same volume fraction. They investigated the effect of the particle size on the mechanical properties of particulate composites at 3 vol% of 0.5mm and 15nm size particles. This study, however, focused on the composites only at low volume fractions. Singh et al. [18] reported that a drastic increase of stiffness of aluminium particle reinforced polyester can be achieved by decreasing the particle size from 20µm to 0.1µm. They also, however, limited to low volume fractions (up to about 2% volume fractions) in their study. In contrast, Liang and Pearson [19] investigated the fracture toughness of two sizes of nanosilica particles (80nm and 20nm) at high volume fractions. They did not, however, compare the mechanical properties of micron sized particles reinforced composites to the nanocomposites. Jang, et al. [20]

investigated the particle size effect on Young's modulus and CTE of the 10 $\mu$ m, 80nm and 20nm SiO<sub>2</sub> particulate composites at only low volume fractions. Dubnikova et al. [21] showed that the behavior of particle reinforced polypropylene composites had a ductile to brittle transition resulting from the change of particle size. Gent, et al [22, 23] showed that the de-bonding stress at the particle/matrix interface can be increased with the decrease in particle size. He also observed that the stress level associated with matrix cavitation and particle/matrix de-bonding in single glass beads embedded elastomer composites is greater with the decrease in glass bead size. Needleman, et al [24] drew a similar conclusion with Gent based on their numerical study using a cohesive zone model. Despite these considerable efforts, few studies have been conducted on the particle size effect on mechanical and thermal properties of particulate composites over a wide range of the particle volume fractions.

### **1.3 Goals and Thesis Organization**

The first goal of this study is to investigate the size effect on mechanical and thermal properties of micro (10 $\mu$ m) and nano (20nm) sized SiO<sub>2</sub> particulate composites over a wide range of the particle volume fractions. Secondly, the existence of a particle size-dependent "effective particle volume fraction" due to the particle/matrix interphase region in a nanoparticle reinforced composite will be demonstrated.

Chapter 1 introduces the background, motivation and goal of this study. Chapter 2 describes the material, composite fabrication and experimental methods of this work. This chapter also discusses the results of experiments. In Chapter 3, a combined numerical/experimental approach is used to study the effects of the particle/matrix interphase on the Young's modulus of SiO<sub>2</sub> particulate nanocomposites

having nanoparticle reinforcements of different sizes. This chapter also introduces the new models that include an interphase region around the nanoparticle which results in an “effective particle volume fraction” that is larger than the actual particle volume fraction. Finally, all results will be then summarized and discussed again in Chapter 4.

## Chapter 2

### MECHANICAL AND THERMAL PROPERTIES OF PARTICULATE POLYMER COMPOSITES

#### 2.1 Material & Composite Fabrication

In order to investigate the effect of particle size on mechanical and thermal properties, particulate composites with the addition of micro- or nano size SiO<sub>2</sub> particles are fabricated.

##### 2.1.1 Material

Micro sized SiO<sub>2</sub> particulate composites are fabricated with diglycidylether of bisphenol A (DGEBA) epoxy as a matrix, and spherically-shaped, 10 μm sized SiO<sub>2</sub> particles (dimension), which were obtained from ABC nanotech Inc. (South Korea) as the filler material. Nano sized SiO<sub>2</sub> particulate composites are also fabricated by using the commercially available standard Nanopox F400 (Nanoresins AG, Germany); spherically shaped, 20 nm SiO<sub>2</sub> particles were supplied as a colloidal silica sol in the resin matrix.

##### 2.1.2 Composite Fabrication

Figure 2.1 shows a schematic of the composite fabrication process. All samples were fabricated by using the matrix material along with the curing agent of Albidur HE600 at a weight ratio of 100:58 according to the supplier. Nanopox F400, DGEBA and Albidur HE600 were supplied by Nanoresins AG (Germany). For particle

dispersion of both micro and nano size  $\text{SiO}_2$  particulate composites, a high speed mechanical shear mixer (Speed Mixer DAC150 FV-K) was used.

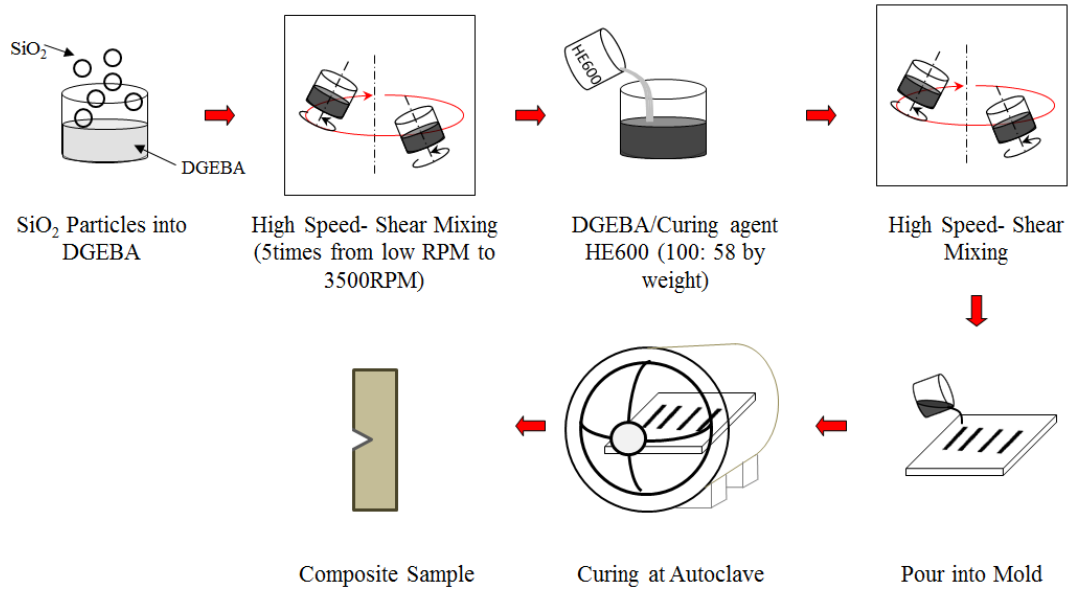


**Figure 2.1:** A schematic illustration of composite fabrication process

All samples were cured in the autoclave with a uniform pressure of 90psi for about 2 hours at 120°C and then 6 hours at 160°C for post curing according to the supplier's recommendation as seen in Figure 2.2. For the tensile test, 10 $\mu\text{m}$  and 20nm  $\text{SiO}_2$  particulate composite samples were fabricated at various particle loadings (up to 15% volume fraction) with sample dimensions following ASTM D638 [27] Type 4, respectively. In order to obtain the fracture toughness, fracture test samples were fabricated following ASTM D5045 [28] for sample dimensions.

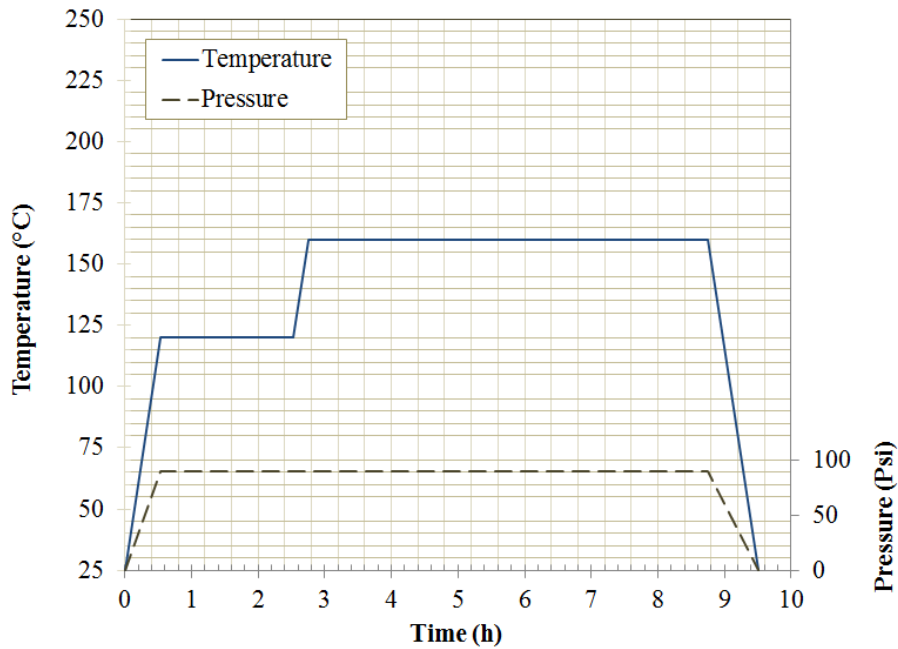


**Figure 2.2:** Sample cure condition of the 20nm and 10 $\mu$ m SiO<sub>2</sub> particulate composites

In order to ensure that the samples are fully cured, the differential scanning calorimeter (DSC; METTLER-DSC1) characterization was performed. The sample (10mg) was heated to 175 °C (beyond  $T_g$  of the matrix) at a rate of 5°C/min, and then cooled down to 25 °C. The sample was then heated again to 175 °C. Identical heat flow curves obtained from the first and second runs can indicate that a sample is fully cured. DSC characterization was performed for all the samples investigated in this work to check the degree of cure of each sample.

Scanning electron microscopy (SEM; JSM-7400F) was used to examine the morphology of fracture surfaces of the particulate composites and particle dispersion quality of the 10 $\mu$ m SiO<sub>2</sub> particulate composites. Since SEM is found not to be an appropriate characterization to examine the nanoparticle distribution and

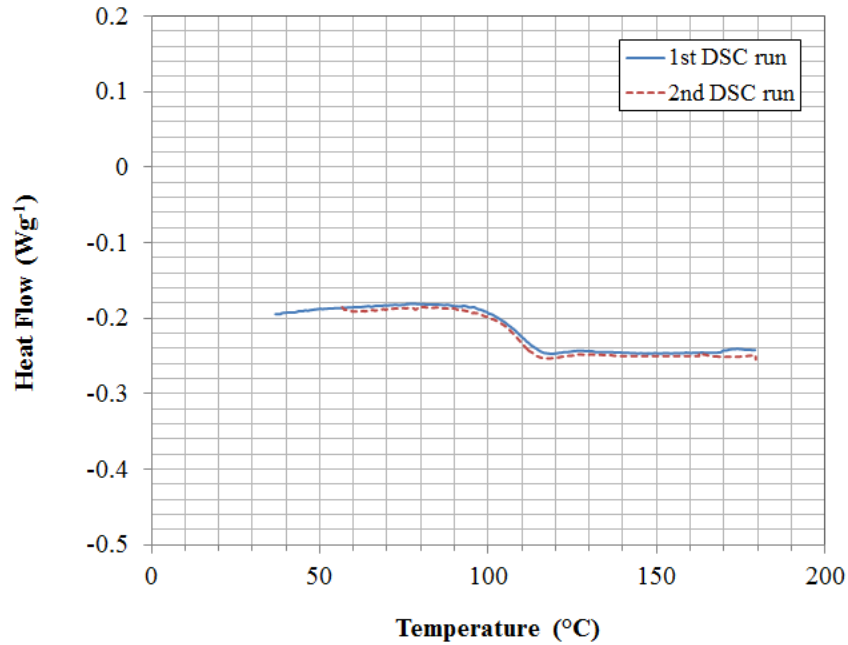
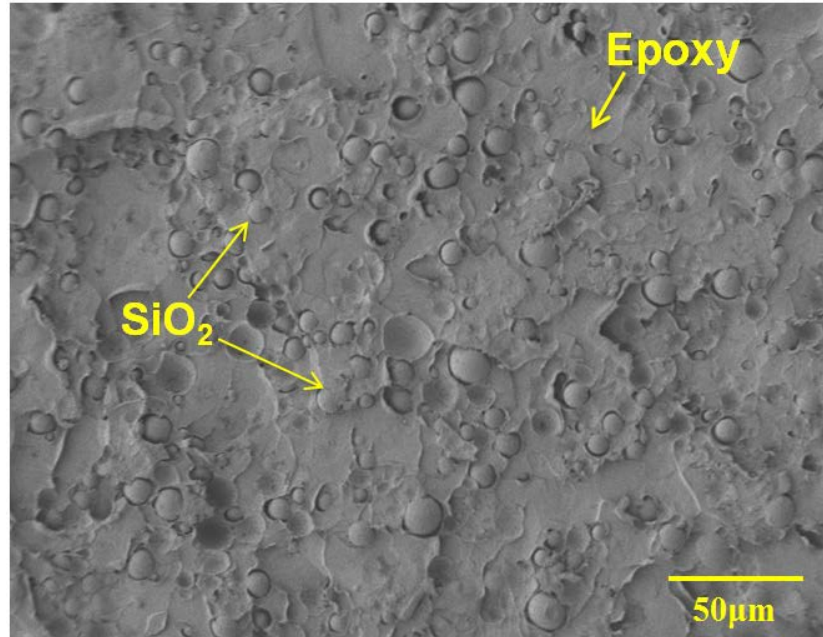


**Figure 2.3:** Results of DSC characterization of neat epoxy

dispersion quality of nanoparticle reinforced epoxy composites, transmission electron microscopy (TEM; 2000fx) was used for 20nm SiO<sub>2</sub> particulate composites. The SEM and TEM characterizations confirmed that all of the samples had reasonably uniform distribution and dispersion quality of the SiO<sub>2</sub> particles in the epoxy matrix. Figure 2.4 (a) shows an SEM image of the fracture surface of 15% volume fraction (highest volume) of 10µm SiO<sub>2</sub> particulate composites and (b) shows TEM images of 15% volume fraction (highest volume) of 20nm SiO<sub>2</sub> particulate composites, respectively.

(a)



(b)

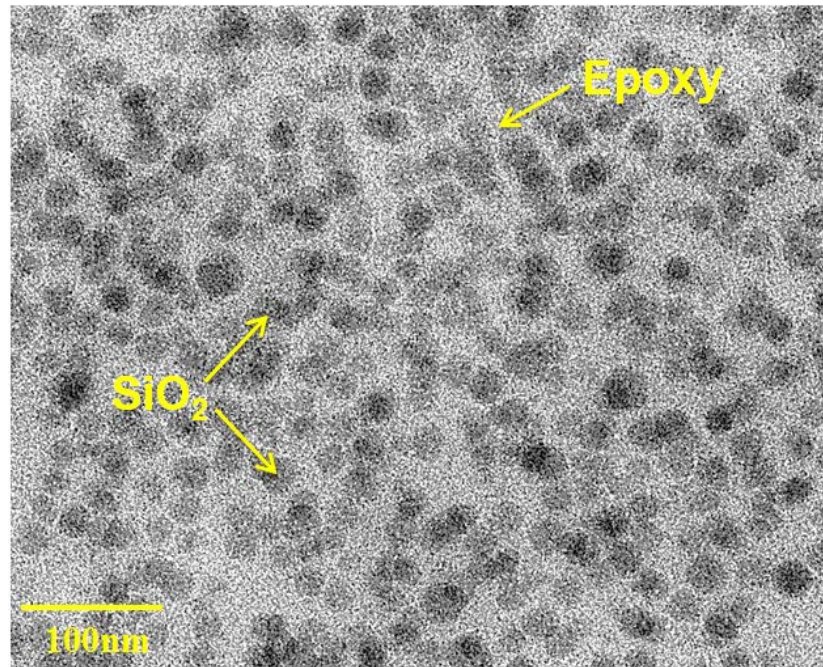


**Figure 2.4:** (a) SEM images of fracture surface of 15vol % of  $\text{SiO}_2$  ( $10\mu\text{m}$ ) particulate composites (b) TEM images of 15vol % of  $\text{SiO}_2$  ( $20\text{nm}$ ) particulate composites at higher magnification

## 2.2 Experimental, Results & Discussion

### 2.2.1 Measurement of Glass Transition Temperature

The glass transition temperature,  $T_g$ , of the samples was measured using DSC. The sample was heated to 170 °C (beyond  $T_g$  of matrix) at a rate of 5°C/min, and then cooled to 25 °C. Dynamic mechanical thermal analysis (DMA) was also performed for each sample, which have dimensions of 30mm in length, 10mm in width, 3mm in thickness, in the single cantilever mode at a test frequency of 1 Hz. The glass transition temperature was determined and was taken to be the temperature at which the peak value of the  $\tan \delta$  occurred. A  $T_g$  of 114°C and 118°C were measured with DSC and DMA, respectively, for the neat epoxy, as shown in Table 2.1. Note that DMA results show higher  $T_g$  values than those obtained by using DSC, as reported by Johnsen et al. [1] and Zhang et al. [12].

**Table 2.1:** Glass transition temperature of the particulate composites at various volume fractions up to 15% of 20nm and 10 $\mu$ m SiO<sub>2</sub> particles

Vol (%)	10 $\mu$ m SiO <sub>2</sub>		20nm SiO <sub>2</sub>	
	DSC (°C)	DMA (°C)	DSC (°C)	DMA (°C)
0	114	118	114	118
1	110	117	120	119
2.5	111	115	123	121
5	107	116	126	126
10	105	116	127	135
15	102	115	128	138

According to the results obtained by DSC, it can be seen that the  $T_g$  of 15vol% 10 $\mu\text{m}$  SiO<sub>2</sub> particulate composite declined by 10.5% from the  $T_g$  of neat epoxy. In contrast, the  $T_g$  of the 15vol% 20nm SiO<sub>2</sub> particulate composite increased by 12% from the  $T_g$  of neat epoxy. These similar trends are also shown in the DMA results. Its origin has not been clearly understood. However, some assumptions are that these behaviors came from the interphase properties between particle and matrix [29] and extra free volume at nanofiller-resin interface [30].

### 2.2.2 Measurement of Coefficient of Thermal Expansion

In order to investigate the CTE behavior of the particulate composites, thermal strain measurements were made using thermo-mechanical analysis (TMA; METTLER TMA/SDTA 841). The linear thermal expansion was determined from room temperature to 80°C (below  $T_g$  for the matrix material). The CTE measurements were conducted using equation (1) from ASTM D 696 [31].

$$CTE = \alpha = \frac{\Delta L}{L_o \Delta T} \quad (1)$$

where  $\Delta L$  is the change in length of the test specimen due to heating,  $L_o$  is the initial length of the test specimen at room temperature, and  $\Delta T$  is the temperature difference over which the change in the length of the specimen is measured. At least 3 samples of each composite were tested to evaluate the CTE. The results presented in Figure 2.5 are the average responses of those samples.

As shown in Figure 2.5, all the composites exhibit a linear strain response in the temperature range. The CTE is decreased with increasing SiO<sub>2</sub> particle volume fraction in the 20nm- and 10 $\mu\text{m}$  SiO<sub>2</sub> particulate composites. Indeed, 20nm SiO<sub>2</sub>

particulate composites show lower CTE values compared to the 10 $\mu$ m SiO<sub>2</sub> particulate composites at all the volume fractions.

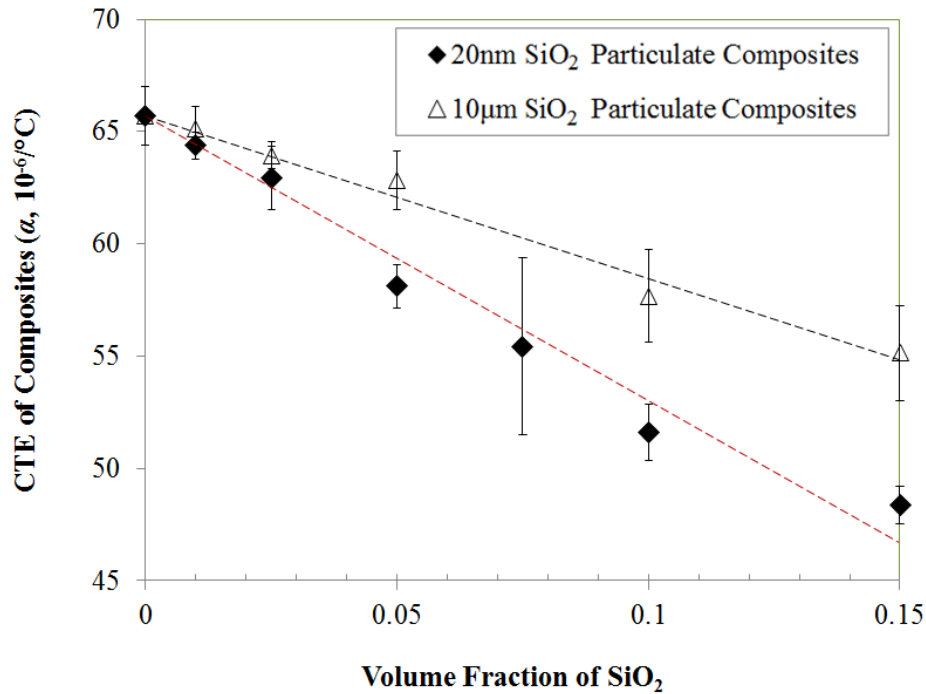


**Figure 2.5:** Experimentally determined CTE of the particulate composites at various volume fractions of 20nm and 10 $\mu$ m SiO<sub>2</sub> particles

The CTE of the particulate composites with 15vol% of 20 $\mu$ m SiO<sub>2</sub> was measured around  $48.3 \times 10^{-6}/^{\circ}\text{C}$  while the CTE of the neat epoxy was measured at  $65.7 \times 10^{-6}/^{\circ}\text{C}$ , which shows a nearly 26.4% reduction in the CTE. Also, The CTE of the particulate composites with 15vol% of 10 $\mu$ m SiO<sub>2</sub> was measured around  $55.1 \times 10^{-6}/^{\circ}\text{C}$ , which indicates a nearly 16.1% reduction in the CTE when compared to the neat epoxy sample.

Generally, this effect can be attributed to the considerably smaller CTE value of the SiO<sub>2</sub> particle (CTE=0.5 x 10<sup>-6</sup>/°C [20]) in comparison to the significantly higher CTE of neat epoxy (CTE=65.7 x 10<sup>-6</sup>/°C). Moreover, the CTE might be also affected by the degree of interphase properties at the vicinity of the particle/ matrix interface [15,32]. Since nanoparticles have significantly large specific surface areas than micro particles at the same volume fraction, the lower CTE of 20nm SiO<sub>2</sub> particulate composites than the CTE of 10µm SiO<sub>2</sub> particulate composites might be induced [33].

### **2.2.3 Measurement of Young's Modulus**

All tensile tests were conducted using an Instron test machine (ElectroPuls E3000) according to ASTM standard D638 [27]. The machine was run under displacement control mode at a cross-head speed of 1mm/min as a quasi-static condition. The cross head displacement was used for strain measurement on the specimen. At least 5 samples of each composite were tested to evaluate the Young's modulus. The Young's modulus was calculated by dividing the tensile stress by the tensile strain in the elastic portion of the stress-strain curve. Figure 2.6 shows the strain- stress curves for 10µm and 20nm SiO<sub>2</sub> particulate composites at various volume fractions.

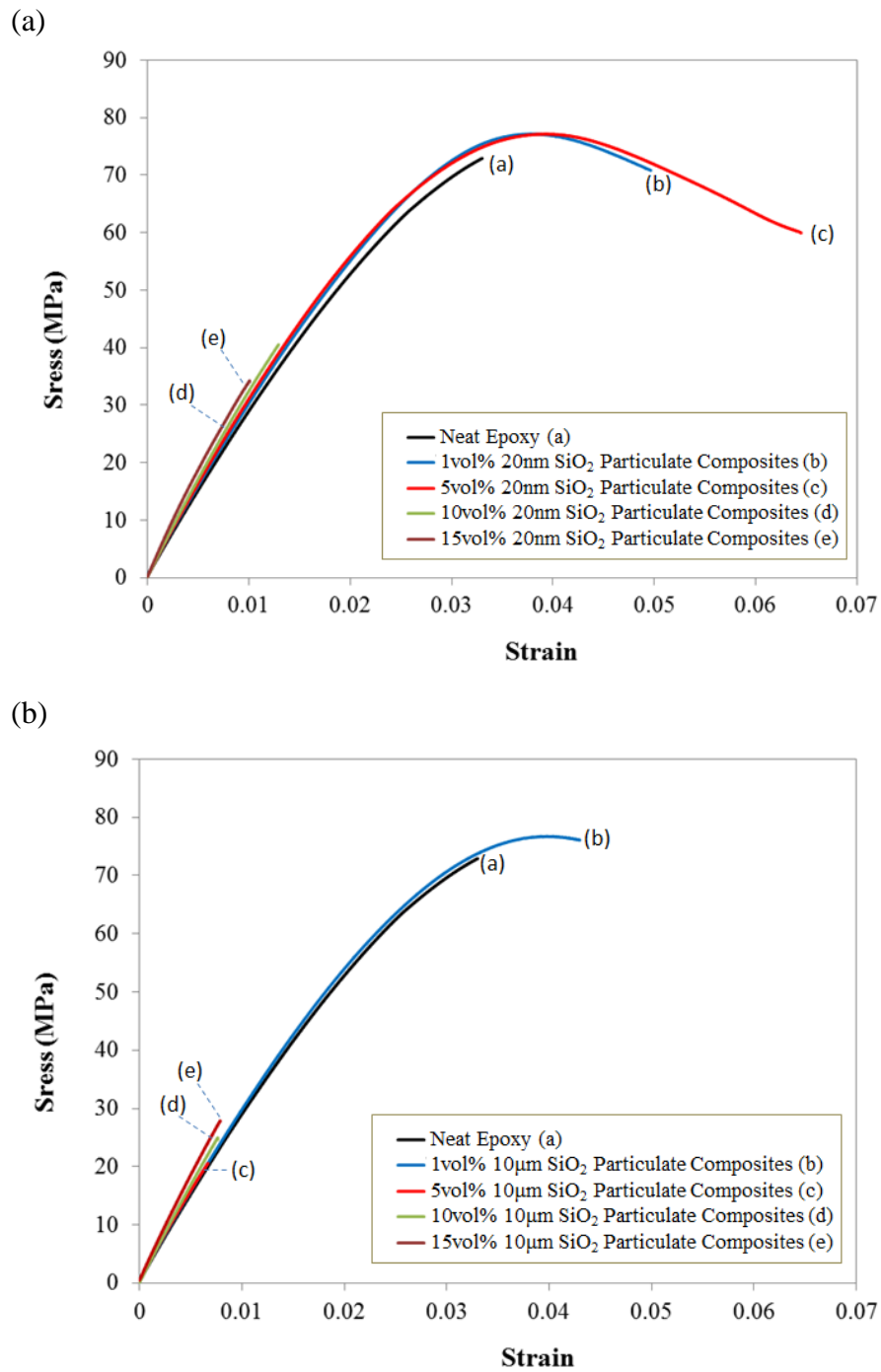


**Figure 2.6:** Stress-strain curves of (a) the 20nm SiO<sub>2</sub> particulate composites at various volume fractions and (b) 10µm SiO<sub>2</sub> particulate composites at various volume fractions

A linear increase in the Young's modulus of 10 $\mu$ m and 20nm SiO<sub>2</sub> particulate composites with respect to the particle loading fraction is seen in Figure 2.7. The results presented are the average responses of those samples. Note that the experimental errors stayed within 3% of the mean values. Young's modulus of the 20nm SiO<sub>2</sub> particulate composite samples with 15vol % was measured to be around 3.78 GPa, showing a 23.5% improvement over that of the neat epoxy (3.06 GPa) while the Young's modulus of the composite samples with 15vol % of 10 $\mu$ m SiO<sub>2</sub> particles was measured to be around 3.58 GPa, showing a 16.9% improvement over that of the neat epoxy. The Young's modulus of the 20nm SiO<sub>2</sub> particulate composites was 5.6% greater than the 10 $\mu$ m SiO<sub>2</sub> particulate composites at the same volume fraction. This clearly shows particle size effects on the Young's modulus of particulate composites. Similar results were reported in earlier works in the introduction [17,18,20]. Recently, there is growing evidence from nanocomposites research that particle size effects may be due at least in part to the fact that the interphase becomes more important as particle size is reduced from the micron range to the nanometer range [20,33].

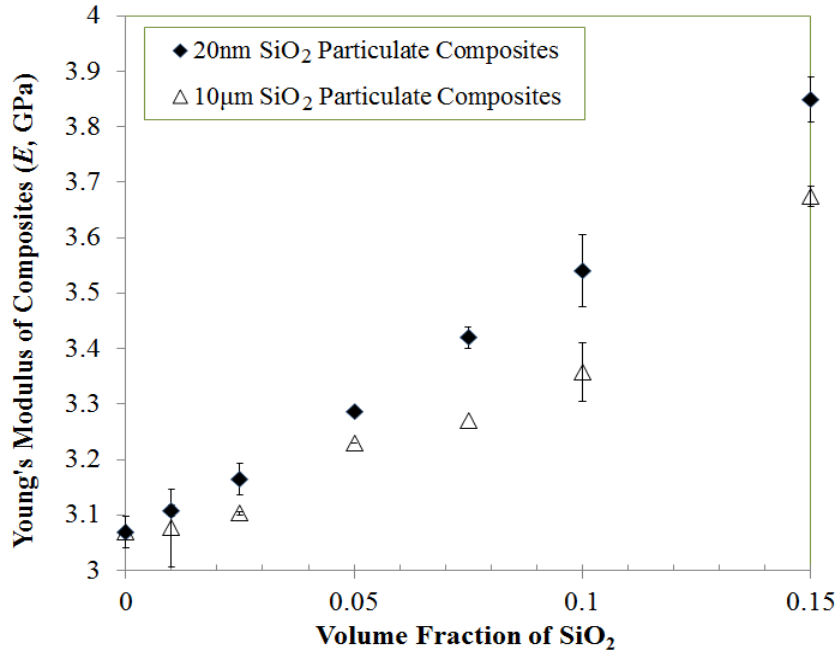


**Figure 2.7:** Experimentally determined Young's modulus of the particulate composites at various volume fractions of 20nm and 10µm SiO<sub>2</sub> particles

#### 2.2.4 Measurement of Tensile Toughness

The tensile toughness was obtained as area under the stress - strain curve. Figure 2.8 shows the tensile toughness of 20nm- and 10µm SiO<sub>2</sub> particulate composites. As shown in Figure 2.8, the tensile toughness of the 20nm SiO<sub>2</sub> particulate composite samples with 1vol % was measured to be around 2.96 MPa, showing a 87.3% improvement over that of the neat epoxy, while the tensile toughness of the composite samples with 1vol % of 10µm SiO<sub>2</sub> particles was measured to be around 2.78 MPa, showing a 75.9 % improvement over that of the neat epoxy. The tensile toughness of the 20nm size SiO<sub>2</sub> particulate composites was 6.5% greater than the 10µm size SiO<sub>2</sub> particulate composites at the 1vol% fraction. The tensile toughness of the 10µm sized SiO<sub>2</sub> particulate composite samples was increased by the addition of

SiO<sub>2</sub> particle until 1vol% and it was decreased after 1vol%. The tensile toughness of the 20nm sized SiO<sub>2</sub> particulate composite samples was increased by the addition of SiO<sub>2</sub> particle until 5vol %, at which the maximum value of 4.6 MPa was measured, showing 191.1% improvement over that of the neat epoxy (1.58 MPa).

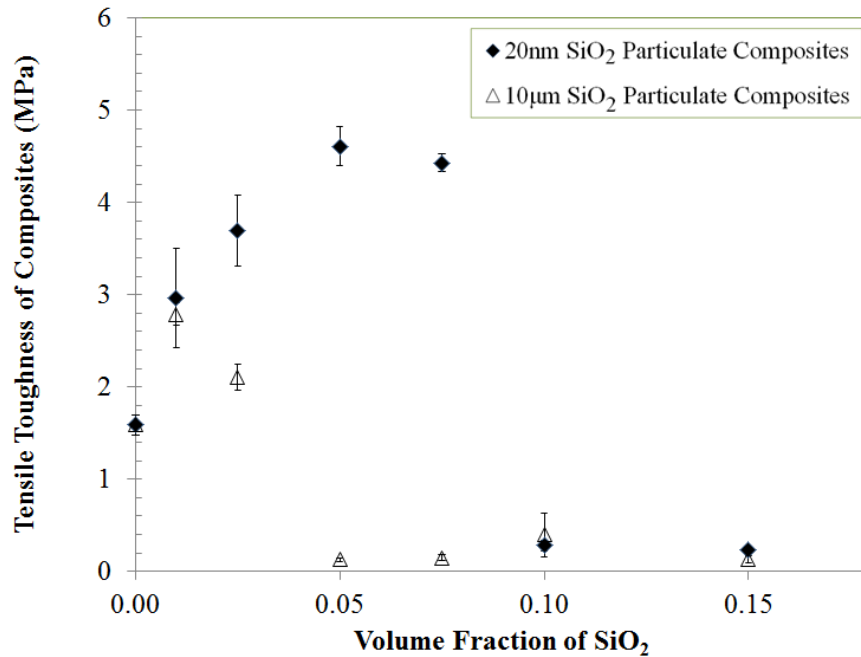


**Figure 2.8:** Experimentally determined tensile toughness of the particulate composites at various volume fractions of 20nm and 10µm SiO<sub>2</sub> particles

### 2.2.5 Measurement of Fracture Toughness

For measurements of fracture toughness, single edge-notched bending (SENB) was used according to ASTM D5045. A sufficiently sharp crack was introduced to the sample by tapping a razor blade. Tapping a razor blade on samples initiates instantly propagated cracks, which are sufficiently sharp for the fracture toughness test. Consequently all the specimens failed by unstable crack growth, and hence only a

single initiation value of the fracture toughness was obtained from each specimen. Ten specimens were tested for each set of data with a crosshead speed of 0.5 mm/sec.

The  $K_{IC}$  values were determined using the equation (2) [28]

$$K_{IC} = \left( \frac{P_Q}{BW^{0.5}} \right) f(a/W) \quad (2)$$

where  $K_{IC}$  is a fracture toughness,  $f$  is the shape factor,  $P_Q$  is the peak load,  $H$  is the specimen thickness (5mm),  $S$  is the span length,  $W$  is the specimen width (5mm) and  $a$  is the crack length.

Tests were performed at room temperature. In the results of the fracture tests, 20nm and 10 $\mu$ m particulate composites showed different fracture toughness,  $K_{IC}$ , at the same volume fraction as shown in Figure 2.9. Different trends were also obtained, in which the toughness of 20nm sized particulate composites reaches a maximum value at 5vol% and decreased beyond 5vol%. Similar results were also seen in Singh et al.'s study [18].

In the results, the fracture toughness of 20nm SiO<sub>2</sub> particulate composites was increased by the addition of SiO<sub>2</sub> particles until 5vol%, at which the maximum  $K_{IC}$  of 1.47 MPa m<sup>1/2</sup> was measured, showing a 72.9% improvement over that of the neat epoxy (0.85 MPa m<sup>1/2</sup>), while the fracture toughness of the micro particulate composites showed only a minor increase by the addition of 10 $\mu$ m SiO<sub>2</sub> particles. The maximum  $K_{IC}$  of 1.05 MPa m<sup>1/2</sup> was measured at 10 vol%, showing a 23.5% improvement over that of the neat epoxy. Note that the experimental errors stayed within less than 40%.

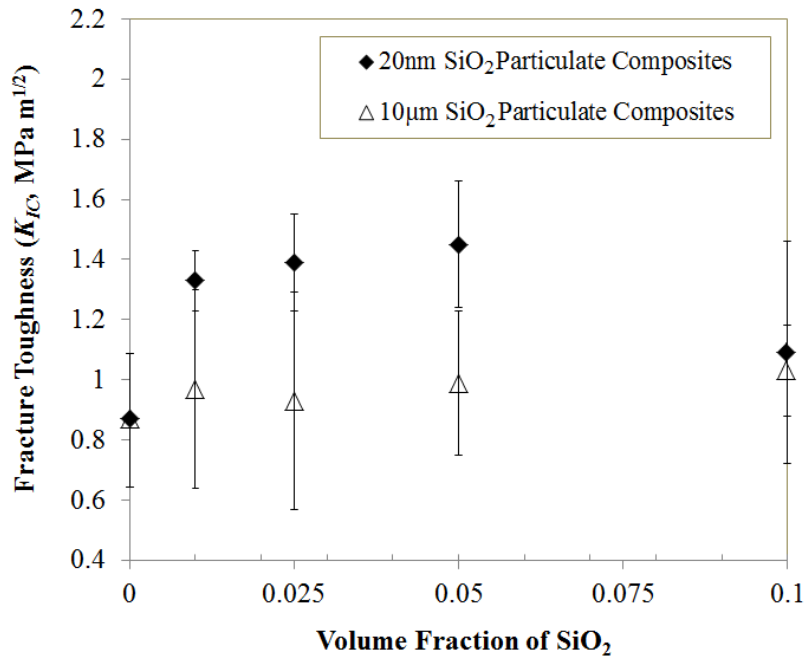


**Figure 2.9:** Experimentally determined fracture toughness of the particulate composites at various volume fractions of 20nm and 10µm SiO<sub>2</sub> particles

The value of the fracture energy,  $G_{IC}$ , was converted from the measured  $K_{IC}$  and Young's modulus, and Poisson's ratio, by using equation (3) for elastic materials since fracture toughness of materials is directly dependent on the energy dissipation. The expressions for  $K_{IC}$  and its relation to  $G_{IC}$  are originally derived for homogeneous and isotropic materials [34].

$$G_{IC} = \frac{K_{IC}^2}{E} (1 - \nu^2) \quad (3)$$

where,  $E$  is the composite's Young's modulus and  $\nu$  is Poisson's ratio of the composites. For  $E$ , the values which were measured by the tensile testing were used, and  $\nu$ , Poisson's ratio, was estimated using the rule of mixture [24] (4).

$$\nu_c = \nu_f V_f + \nu_m (1 - V_f) \quad (4)$$

where  $V_f$  is the filler volume fraction, and the subscripts  $c$ ,  $m$ , and  $f$  refer to composite, matrix and filler. Values of 0.35 and 0.175 were used for Poisson's ratio of the matrix and filler ( $\text{SiO}_2$ ), respectively.

The results are shown in Figure 2.10. According to the results, the fracture energy of the nano-composite samples with 5vol % of  $\text{SiO}_2$  particles was measured to be approximately  $0.561 \text{ KJ/m}^2$ , showing a 162.1% improvement over the neat epoxy ( $0.214 \text{ KJ/m}^2$ ), while the fracture energy of the micron composite samples with 5vol % of  $\text{SiO}_2$  particles was measured to be about  $0.266 \text{ KJ/m}^2$ , showing only a 24.2% improvement over the neat epoxy. It was observed that both  $K_{IC}$  and  $G_{IC}$  values increase with a decrease in  $\text{SiO}_2$  particle size. These results can indicate that the effect of particle size on fracture toughness for the particulate composite is significant.

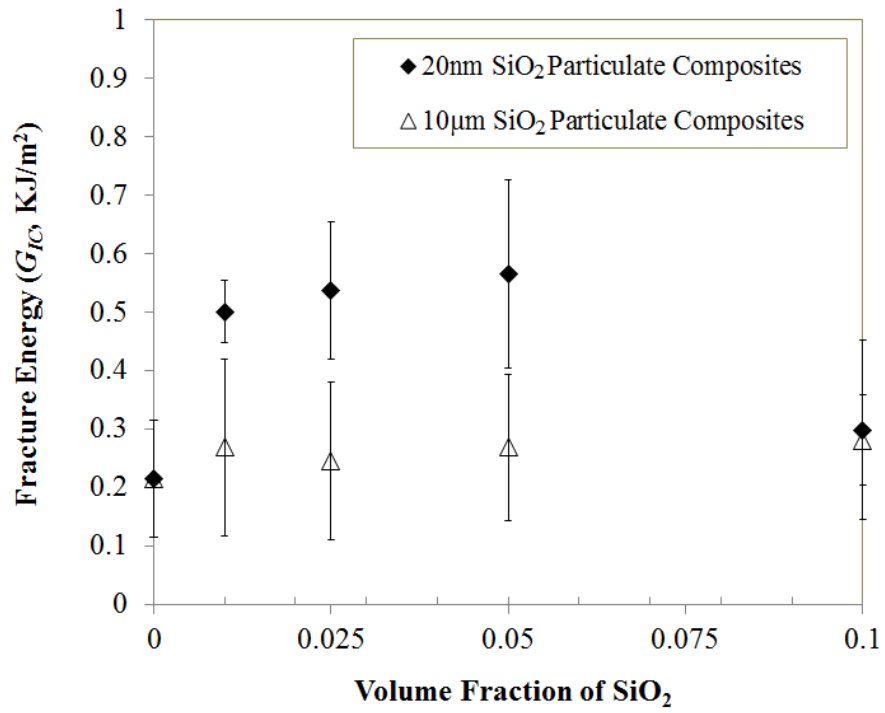


**Figure 2.10:** Fracture energy of the particulate composites at various volume fractions of 20nm and 10µm SiO<sub>2</sub>

## **Chapter 3**

### **A PARTICLE SIZE-DEPENDENT “EFFECTIVE PARTICLE VOLUME FRACTION”**

Our experiments showed that the mechanical properties of the composites increase and the CTE of the composites decrease with decreasing particle diameter in Chapter 2. As discussed earlier, these mechanical and thermal properties are induced by different interphase regions around the particles along with particle size. However, the material properties and size of the interphase regions are not clear.

So far, many researchers have developed micromechanics models to predict the material properties of composites [35-47]. For example, based on the rigid particle assumption, Einstein's equation [35,36] can predict the Young's modulus of particulate composites. Halpin and Tsai [40] also found that the modulus of particulate composites can be predicted. Counto [47] proposed a simple model for a two phase particulate composite by assuming perfect bonding between filler and matrix for composite modulus. The size effect of mechanical and thermal properties of composites, however, cannot be expected by using these micromechanics models since they are no consideration of particle size. Therefore, the new models include an interphase region around the nanoparticle which results in an “effective particle volume fraction” that is larger than the actual particle volume fraction.

#### **3.1 Interphase Region for Size Effect**

The interphase concept has been used in several studies (Cannillo, et al. [48], and Liu and Brinson [49]) in order to accurately model the experimental results for stiffness of nanocomposites. Vo, et al. [50] was among the first to investigate the

effects of the interphase on the modeling of particle-reinforced composites by fitting various closed form models to experimental data for composites composed of micron-sized  $\text{Al}_2\text{O}_3$  particles in a silver matrix. Brown, et al. [51] used molecular dynamics simulations to show that the interphase thickness in polymer nanocomposites was independent of particle size. Therefore, for a fixed particle volume fraction, reduced particle size can lead to an increasing influence of the interphase on overall composite behavior.

As with conventional fiber composites, several different models for interphase property gradients have been assumed in the modeling of particulate composites and nanocomposites. For example, Voros and Pukanszky [52,53] assumed that the elastic properties of the interphase in particulate composites varied according to a power law function of radius in the calculation of stresses and displacements around the particle. Dominkovics, et al. [54] assumed a constant property distribution across the interphase in order to estimate the interphase thickness and composite properties in layered silicate-reinforced nanocomposites. Qiao and Brinson [55] found that a two-layer interphase model was more effective than a single layer model in explaining the behavior of the loss modulus and the loss tangent of polymer nanocomposites. Cannillo, et al. [48] assumed a constant Young's modulus across the interphase thickness in developing finite element models of ceramic particle filled polymer matrix composites. Boutaleb, et al. [56] assumed a power law modulus gradient across the interphase thickness in finite element models of silica/polymer nanocomposites. Dong and Bhattacharyya [57] developed finite element models of polypropylene/organoclay nanoplatelet composites assuming a single layer interphase having a uniform modulus,  $E_i$ , of either  $E_i = 0.5 E_m$ ,  $E_m$  or  $2.0 E_m$ , where  $E_m$  is the matrix

modulus. Li, et al. [58] reported on closed form elasticity models of nanocomposites assuming a single layer interphase having  $E_i = 3.0 E_m$ .

In summary, it seems that a variety of assumptions have been made regarding interphase property modeling, and currently there is no clear understanding of the best way to model interphase property gradients in nanocomposites. The assumptions made, however, in our current work will hopefully provide useful insight and design guidelines for nanocomposites.

### 3.2 The Concept of Effective Particle Volume Fraction

The concept of an “effective volume fraction” is central to the modeling approach employed in this study. The interphase region may develop at the particle/matrix interface due to partial immobilization of the polymer matrix near the interface. This interphase region leads to an “effective volume fraction” of reinforcement which is larger than the actual volume fraction of reinforcement. For example, for a spherical particle and its surrounding interphase having the dimensions shown in Figure 3.1, the ratio of the effective particle volume fraction,  $v_{eff}$ , to the actual particle volume fraction,  $v_{act}$ , is given by

$$\frac{v_{eff}}{v_{act}} = \left(1 + \frac{\Delta R}{R}\right)^3 \quad (5)$$

where  $R$  is the particle radius and  $\Delta R$  is the interphase thickness.

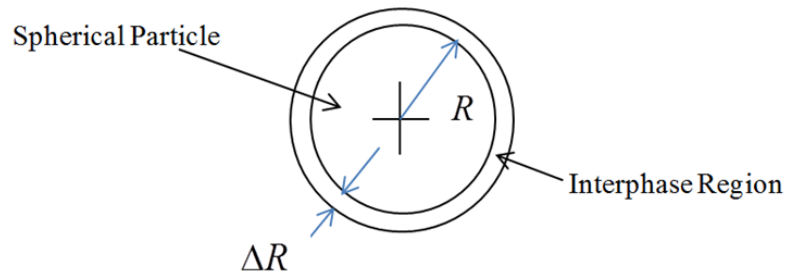


**Figure 3.1:** Spherical particle surrounded by interphase region

Experimental evidence suggests that as  $R$  is reduced from the micron range to the nanometer range,  $\Delta R/R$  and  $v_{eff}/v_{act}$  increase. For example, Zhang, et al. [58], reported that for nanosilica/epoxy nanocomposites,  $\Delta R/R$  was in the range of 0.22-0.84, which is an order of magnitude larger than that of microparticle-filled composites, which is in the range 0.02-0.07. This obviously has important implications for analytical modeling of nanocomposites. It will be shown in this chapter that finite element models including the interphase are better able to predict the experimentally determined Young's modulus of silica/epoxy composites as the particle size is reduced from the micron range to the nanometer range.

### 3.3 Finite Element Modeling

The finite element model designed for this study will be described in this part. Each part of the finite element design, from the geometry to the boundary conditions, will be explained. The Young's modulus calculation methods also will be presented.

### 3.3.1 Geometry of the Model

3D finite element analysis models have been selected for this study. Since the number of particles in the model does not have a significant effect at the same volume fraction [60], the single particle representative volume element (RVE) model was used. In this study, two different particle diameters were investigated to be able to match with the experimental data: 10  $\mu\text{m}$  and 20 nm. For each particle size, 1%  $\text{SiO}_2$  particle volume fraction was studied for Young's modulus experimental data. The required length of the cubic side is calculated for a given particle diameter and particle volume fraction. The cubic side lengths are shown in Table 3.1 for Young's modulus for each combination of particle size and particle volume fraction. The model includes only particle and matrix material, but as indicated earlier, another material must be included between the particle and the matrix as well. This third material is the "interphase region" (Figure 3.1). It represents the effect of the particle/matrix interaction; its thickness depends on the particle diameter and will be used as a curve-fitting parameter in the model described later.

**Table 3.1:** Length ( $\mu\text{m}$ ) of the cubic side for 10 $\mu\text{m}$  and 20nm size particles for 1% volume fraction

Particle diameter	Length ( $\mu\text{m}$ ) of the cubic side
10 $\mu\text{m}$	37.4
20 nm	0.0748

### 3.3.2 Mechanical Properties and Interphase Model

The material properties of the particle and the matrix are given in Table 3.2 from [1,60]. Two material properties for each material are essential to complete the FE study: Young's modulus and Poisson's ratio. Since the material properties of the interphase are unknown, linear property gradient approximations for the interphase will be assumed in this study.

**Table 3.2:** Material properties of particle and matrix [1,60]

Material Properties	Material	Particle	Matrix
		SiO <sub>2</sub>	DGEBA
Young's Modulus (MPa)		70000	3069
Poisson's ratio		0.17	0.35

As previously discussed in Chapter 3.1, a variety of assumptions have been reported in the literature regarding the distribution of properties (Young's modulus and Poisson's ratio) across the thickness of the interphase in both conventional fiber composites and more recent nanocomposites. Unfortunately, there seems to be no clear guidance as to which approach is best. The approach chosen here is to assume that the properties in the interphase region vary linearly across the interphase thickness, from the property of the particle to that of the matrix. To simplify the FE model for this case, the interphase region is divided into three sections (Figure 3.2), with each section containing different material properties.

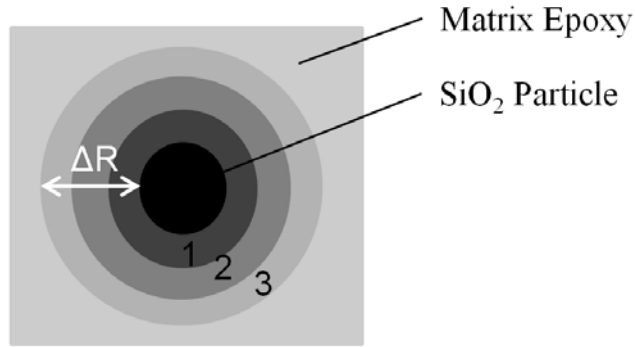


**Figure 3.2:** Simplified: the interphase region is divided into three sections to approximate the linear variation of properties across its thickness

In order to obtain the material properties in the three sections as shown in Table 3.3, a linear distribution of properties across the interphase and equal thicknesses in each of the three interphase sections are assumed.

**Table 3.3:** Interphase region properties (simplified)

Interphase Region / Material Properties	Section 1	Section 2	Section 3
Young's Modulus (MPa)	58844.8	36534.5	14224.1
Poisson's ratio	0.2	0.26	0.32

### 3.3.3 Elements, Meshing and Boundary Conditions

The element used for meshing in ANSYS was a simple 3D 8-node brick element (Figure 3.3). It has a minimum number of nodes to save computational

resources and is accurate enough for this kind of simple model. Each node has three degrees of freedom in the displacements:  $U_x$ ,  $U_y$ ,  $U_z$ . As shown in Figure 3.4, a 1/8 domain section is used to take advantage of the double symmetry of the single particle representative volume element (RVE). Three faces of the cube along the planes  $X=0$ ,  $Y=0$  and  $Z=0$  are constrained against deformations perpendicular to their initial positions, while the deformations of the three other faces are defined with the multi-point constraint. Multi-point constraint (MPC) is used to constrain every node of each concerned face so that the face deforms parallel to its original undeformed position. The use of MPC insures that there is geometric compatibility between each RVE and its identical neighboring RVE's after deformation [60].

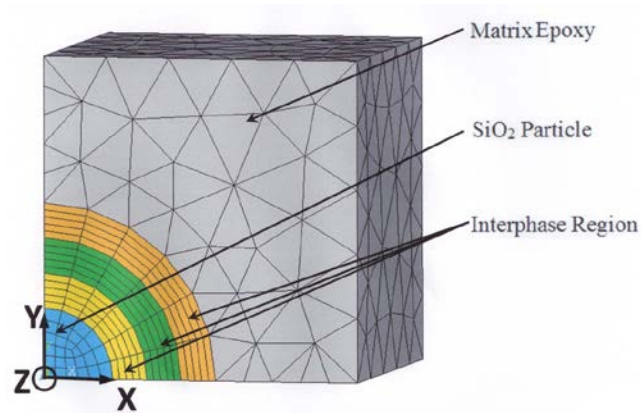


**Figure 3.3:** Typical 3D view of the meshed 1/8 domain finite element model

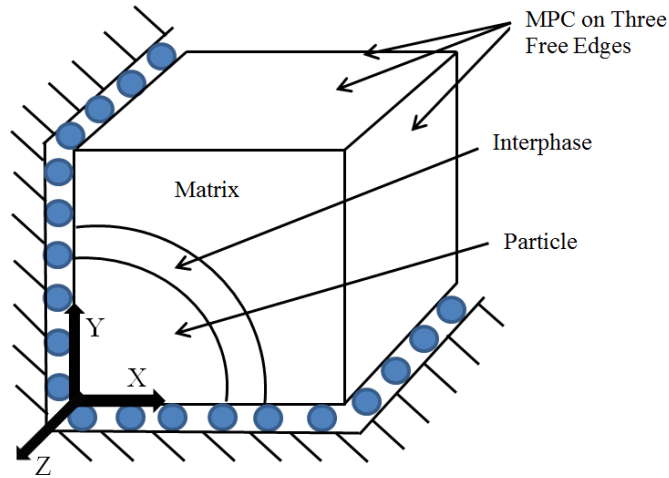


**Figure 3.4:** Roller-slider boundary conditions on planes  $X=0$ ,  $Y=0$ , and  $Z=0$  and Multi-Point Constraint (MPC) on the three other faces of 1/8 domain model

### 3.3.4 Young's Modulus Determination

In order to calculate the Young's modulus, a constant strain was applied on one of the free faces of the RVE. The average stress of all nodes in the opposite side from the applied strain was divided by applied strain.

### 3.3.5 Interphase Region Thickness

For the finite element models with interphase region,  $\Delta R$  is assumed to be a floating value, because at this step the exact thickness of the interphase region is unknown. That is why the experimental Young's modulus data is used for matching with the FE result. In fact,  $\Delta R$  and the resulting  $v_{eff}$  are used as curve-fitting parameters in order to match the FE-predicted Young's modulus with the corresponding experimentally determined values for a composite reinforced with particles of known radius  $R$  and actual particle volume fraction,  $v_{act}$ . Then, for each

case, this procedure follows the evolution of this interphase region thickness for given particle diameters and actual particle volume fractions.

### 3.4 Results & Discussion

For an actual particle volume fraction of 1 %, the FE-predicted and experimental Young's modulus are compared in Figure 3.5. Clearly the FE model "w/o interphase" does not follow the experimental results and does not show any changes in properties with changing particle diameter, while the FE model with an interphase region (i.e., "effective particle volume fraction") reflects the experimentally observed increases in Young's modulus with decreasing particle diameter. These results also clearly show that the presence of the interphase region can explain the experimentally observed increases in Young's modulus while decreasing particle size, whereas the FE models without interphase predict no particle size effect.

When the thickness of the interphase region,  $\Delta R$ , is assumed for a given particle radius  $R$  and particle volume fraction  $v_{act}$ , the ratio  $\Delta R/R$  is fixed and the effective volume fraction,  $v_{eff}$ , can be found from Equation (5). Figure 3.6 shows the evolution of  $\Delta R/R$  and  $v_{eff}$  with particle diameter, for the same case of  $v_{act}=1\%$ . The ratio  $\Delta R/R$  in Figure 3.6 is clearly increasing while particle size decreases, from 0.01 for 10  $\mu\text{m}$  particles to 0.5 for 20 nm particles. At the same time, the effective volume fraction for E increases from 1.1% for 10  $\mu\text{m}$  particles to 3.5% for 20 nm particles, even though the actual particle volume fraction is only 1%. The ratio of interphase thickness to particle diameter and the corresponding effective volume fraction are found to significantly increase with the decrease in particle diameter from the micrometer range to the nanometer range.

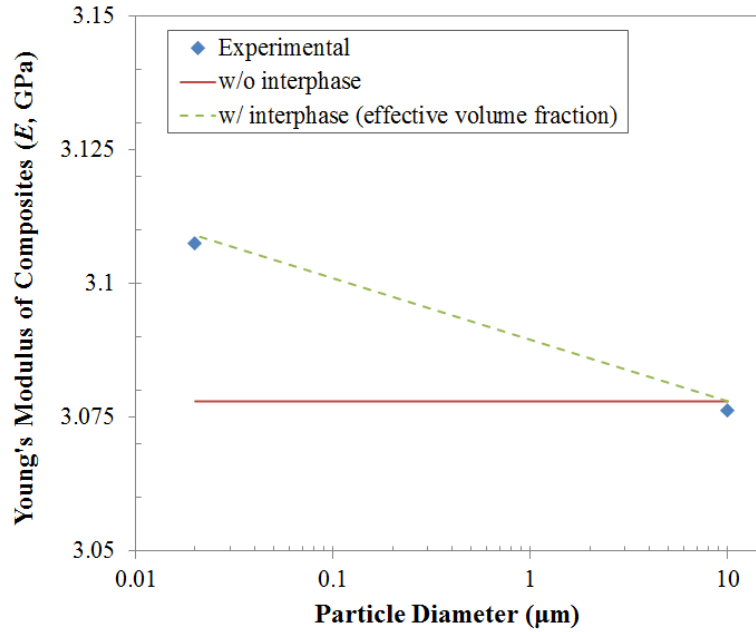


**Figure 3.5:** Calculated results for FE models with and without interphase region compared with experimental values at particle volume fraction of 1 vol%

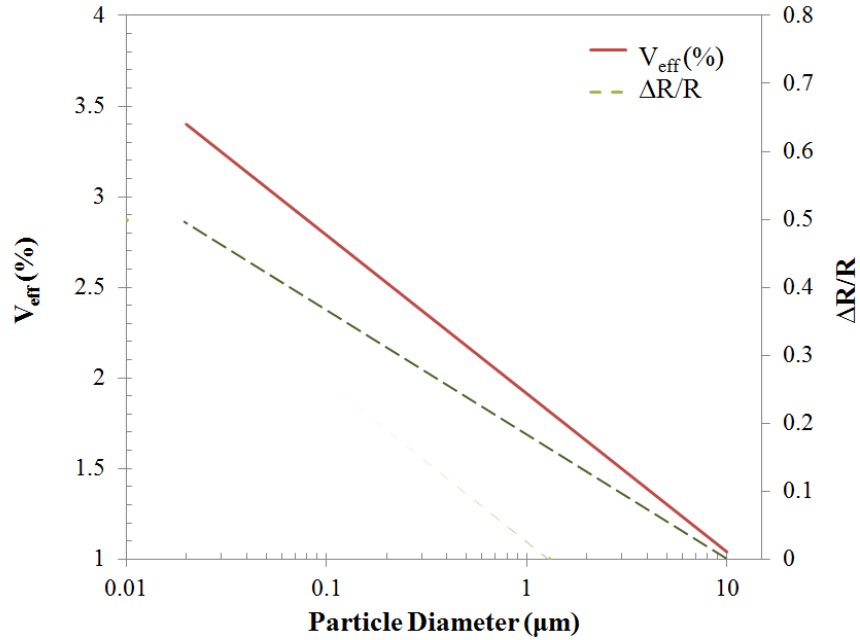


**Figure 3.6:**  $\Delta R/R$  and  $v_{\text{eff}}$  from FE model with interphase region at particle volume fraction of 1 vol%

## Chapter 4

### CONCLUSIONS

In this study, 10 $\mu$ m and 20nm SiO<sub>2</sub> particulate composites were successfully fabricated. Mechanical and thermal properties of both micro- and nano sized SiO<sub>2</sub> particulate composites over a wide range of the particle volume fractions were investigated to understand the particle size effect.

From the experimental results, it is shown that the effect of particle size on mechanical and thermal properties is significant. In the CTE measurement, the CTE of the particulate composites with 15vol% of 20nm SiO<sub>2</sub> was decreased by 26.4% while the CTE of the particulate composites with 15vol% of 10 $\mu$ m SiO<sub>2</sub> showed a 16.1% reduction from the CTE of neat epoxy. Indeed, the Young's modulus of the 20nm sized SiO<sub>2</sub> particulate composite samples with 15vol % showed a 23.5% improvement over that of the neat epoxy, while the Young's modulus of the particulate composite samples with 15vol% of 10 $\mu$ m SiO<sub>2</sub> particles showed a 16.9% improvement over that of the neat epoxy. The tensile toughness of the 20nm sized SiO<sub>2</sub> particulate composite samples with 1vol% showed a 87.3% improvement over that of the neat epoxy, while tensile toughness of the particulate composite samples with 1 vol % of 10 $\mu$ m SiO<sub>2</sub> particles showed a 75.9 % improvement over that of the neat epoxy. The tensile toughness of the 10 $\mu$ m sized SiO<sub>2</sub> particulate composite samples was increased by the addition of SiO<sub>2</sub> particle until 1vol% and it was decreased after 1vol%. The tensile toughness of the 20nm sized SiO<sub>2</sub> particulate composite samples was increased by the addition of SiO<sub>2</sub> particle until 5vol% and showed a 191.1% improvement over that of the neat epoxy. The fracture toughness of 20nm SiO<sub>2</sub> particulate composites was

increased by 72.9% with the addition of SiO<sub>2</sub> particle until 5vol% from neat epoxy, while the fracture toughness of 10µm particulate composites showed little increase by the addition of SiO<sub>2</sub> particles. The fracture energy of the nano-composite samples with 5vol % of SiO<sub>2</sub> particles were converted and showed a 162.1% improvement over the neat epoxy, while the fracture energy of the micron composite samples with 5vol% of SiO<sub>2</sub> particles showed only a 24.2% improvement over the neat epoxy.

Finally, it has been shown that, by including the interphase region in the FE models of particulate nanocomposites and using the interphase thickness  $\Delta R$  for a given particle radius,  $R$ , and the corresponding effective particle volume fraction,  $v_{eff}$ , as a curve-fitting parameter, it is possible to accurately match the experimentally observed enhancement of the Young's modulus of the composite with decreasing particle diameter. Corresponding FE models without interphase showed no change in the Young's modulus of the composite with decreasing particle diameter. The predicted evolution of the ratio  $\Delta R/R$  and the effective particle volume fraction with changing particle diameter and particle volume fraction has been found to be different for the Young's modulus. The ratio of interphase thickness to particle diameter and the corresponding effective volume fraction are found to significantly increase with the decrease in particle diameter from the micrometer range to the nanometer range.

## **FUTURE WORK**

In order to better understand the size effect on the mechanical and thermal properties of particulate polymer composites and also identify their potential applications, further study is necessary. Here, this study suggests following future works:

- 1) Applying the effective volume fraction concept to composites with high volume fraction and to thermal properties of composites.
- 2) Understanding the toughening mechanisms responsible for the improvement in the fracture toughness of nano sized SiO<sub>2</sub> particulate epoxy composites.
- 3) Demonstration of the use of nano sized particle reinforced polymer composites as an advanced adhesive with enhanced energy absorbing capabilities for structural applications.

## REFERENCES

- [1] B.B. Johnsen, A.J. Kinloch, R.D. Mohammed, A.C. Taylor, S. Sprenger, Toughening mechanisms of nanoparticle-modified epoxy polymers, *Polymer* 48(2007) 530-541.
- [2] S.S. Ray, M. Okamoto, Polymer/layered silicate nanocomposites: a review from preparation to processing, *Prog Polym Sci* 28(2003) 1539-1641.
- [2] Alexandre M., Dubois P, Polymer-layered silicate nanocomposites: preparation, properties and uses of a new class of materials, *Mater Sci Eng R* 28(2000) 1-63.
- [3] M.H. Kim, C.I. Park, W.M. Choi, J.W. Lee, J.G. Lim, O.O. Park, Synthesis and material properties of syndiotactic polystyrene/ organophilic clay nanocomposites, *J Appl Polym Sci* 92(2004) 2144-2150.
- [4] L. Liu, Z. Qi, X. Zhu, Studies on nylon 6/clay nanocomposites by melt-intercalation process, *J Appl Polym Sci* 71(1991) 1133-1138.
- [5] A. Usuki, Y. Kojima, M. Kawasumi, A. Okada, Y. Fukushima, T. Kurauchi, Synthesis of nylon-6–clay hybrid, *J Mater Res* 8(1993) 1179-1183.
- [6] E.P. Giannelis, Polymer layered silicate nanocomposites, *Adv Mater* 8(1996) 29-35.

- [7] Y. Kojima, A. Usuki, M. Kawasumi, Y. Fukushima, A. Okada, T. Kurauchi, One-pot synthesis of nylon-6 clay hybrid, *J Polym Sci Part A Polym Chem* 31 (1993) 1755-1758.
- [8] H.L. Tyan, Y.C. Liu, K.H. Wei, Thermally and mechanically enhanced clay/polyimide nanocomposite via reactive organoclay, *Chem Mater* 11 (1999) 1942-1947.
- [9] H. Shi, T. Lan, T. Pinnavaia, Interfacial effects on the reinforcement properties of polymer-organoclay nanocomposites, *Chem Mater* 8 (1996) 1584-1587.
- [10] J.W. Cho, D.R. Paul, Nylon 6 nanocomposites by melt compounding, *Polymer* 42 (2001) 1083-1094.
- [11] Y. Nakamura, M. Yamaguchi, Effect of particle size on the fracture toughness of epoxy resin filled with spherical silica, *Polymer* 33 (1992) 3415-3426.
- [12] H. Zhang, L.C. Tang, Z. Zhang, K. Friedrich, S. Sprenger, Fracture behaviors of in situ silica nanoparticle-filled epoxy at different temperatures, *Polymer* 49 (2008) 3816-3825.
- [13] J. Ma, M.S. Mo, X-S. Du, P. Rosso, K. Friedrich, H-C Kuan, Effect of inorganic nanoparticles on mechanical property, fracture toughness and toughening mechanism of two epoxy systems, *Polymer* 49 (2008) 3510-3523.
- [14] T.H. Hsieh, A.J. Kinloch, K. Masania, A.C. Taylor, S. Sprenger, The mechanisms and mechanics of the toughening of epoxy polymers modified with silica nanoparticles, *Polymer* 51(2010) 6284-6294.

- [15] Hiroshi Hatta, Takako Takei, Minoru Taya, Effects of dispersed microvoids on thermal expansion behavior of composite materials, *Mater Sci Eng A285* (2000) 99–110.
- [16] B.C. Kim, S.W. Park, D.G. Lee, Fracture toughness of the nano particle reinforced epoxy composite, *Composite structures* 86 (2008) 69-77.
- [17] J. Cho, M.S. Joshi, C.T. Sun, Effect of inclusion size on mechanical properties of polymeric composites with micro and nano particles, *Compos Sci Technol* 66 (2006) 1941-1952.
- [18] R.P. Singh, M. Zhang, D. Chan , Toughening of a brittle thermosetting polymer: effects of reinforcement particle size and volume fraction. *J Mater Sci* 37 (2002) 781-788.
- [19] Y.L. Liang, R.A. Pearson, Toughening mechanisms in epoxy-silica nanocomposites (ESNs), *Polymer* 50 (2009) 4895-4905.
- [20] J. Jang, R. F. Gibson and J. Suhr, Characterization of particle diameter and interphase effects on Young's modulus of SiO<sub>2</sub>/epoxy particulate composites, In proceedings of the SPIE Smart Structures/NDE 2012 - Behavior and Mechanics of Multifunctional Materials and Composites, March 11 - 15, 2012, San Diego, CA, USA.
- [21] I.L. Dubnikova, V.G. Osmyan, A. Ya. Gorenberg, Mechanisms of particulate filled polypropylene finite plastic deformation and fracture, *J Mater Sci* 32 (1997) 1613-1622.

- [22] A.N.Gent, Detachment of an elastic matrix from a rigid spherical inclusion. *J Mater Sci* 15 (1980) 2884-2888.
- [23] A.N. Gent, B. Park, Failure processes in elastomers at or near a rigid spherical inclusion, *J Mater Sci* 19 (1984) 1947-1956.
- [24] A Needleman, A continuum model for void nucleation by inclusion debonding. *J Appl Mech* 54 (1987) 531-545.
- [25] J. K. Chen, Z. Hung, J. Zhu, Size effect of particles on the damage dissipation in nanocomposites, *CST* 67 (2007) 2990-2996.
- [26] S. Fu, X. Feng, B. Lauke, Y-W. Mai, Effects of particle size, particle/matrix interface adhesion and particle loading on mechanical properties of particulate – polymer composites, *Composites: Part B* 39 (2008) 933-961.
- [27] ASTM international, Standard Test Method for Tensile Properties of Plastics, Report NO. ASTM D 638 (2008).
- [28] ASTM international, Standard Test Methods for Plane-Strain Fracture Toughness and Strain Energy Release Rate of Plastic Materials, ASTM D5045 (2007).
- [29] KT. Farber, AG. Evans, Crack deflection processes II. Experimental, *Acta Metall* 31 (1983) 577.
- [30] Y. Sun, Z. Zhang, K.-S. Moon, C.P. Wong, Glass transition and relaxation behavior of epoxy nanocomposites, *J Polym Sci Part B Polym Phys* 42 (2004) 3849.

- [31] ASTM international, Standard Test Method for Coefficient of Linear Thermal Expansion of Plastics Between -30°C and 30°C With a Vitreous Silica Dilatometer, ASTM D696 (2008).
- [32] S. Kang, S. Hong, Preparation and characterization of epoxy composites filled with functionalized nanosilica particles obtained via sol-gel process, *Polymer* 42(2001) 879-887.
- [33] L. Sun, R. F. Gibson, F. Gordaninejad, J. Suhr, Energy absorption capability of nanocomposites: A review, *Compos Sci Technol* 69 (2009) 2392-2409.
- [34] ASTM international, Standard Test Methods for Plane-Strain Fracture Toughness and Strain Energy Release Rate of Plastic Materials, ASTM D5045-99 (1999).
- [35] A. Einstein, Ueber die von der molekularkinetischen fluessigkeiten suspendierten teilchen, *Ann Phys (Leipzig)* 17 (1905) 549-560.
- [36] A. Einstein, Investigation on theory of Brownian motion, New York: Dover (1956).
- [37] CH. Hsueh, PF, Becher, Effective viscosity of suspensions of spheres, *J Am Ceram Soc* 88 (2005)1046-1049.
- [38] IH Tavman, Thermal and mechanical properties of aluminum powder-filled high-density polyethylene composites, *J Appl Polym Sci* 62 (1996) 2161-2167.
- [39] E. Guth, Theory of filler reinforcement, *J Appl Phys* 16 (1945) 20-25.
- [40] JC. Halpin, Stiffness and expansion estimates for oriented short fiber composites, *J Compos Mater* 3 (1969), 732-734.

- [41] EH. Kerner, The elastic and thermoelastic properties of composite media. Proc Phys Soc B 69 (1956) 808-813.
- [42] LE. Nielsen, Generalized equation for the elastic moduli of composite materials, J Appl Phys 41 (1970) 4626-4627.
- [43] LE. Nielsen, Dynamic mechanical properties of polymers filled with agglomerated particles, J Polym Sci Polym Phys 17(1979) 1897-1901.
- [44] TB. Lewis, LE. Nielsen, Dynamic mechanical properties of particulate filled composites. J Appl Polym Sci 14 (1970) 1449-1471.
- [45] M. Mooney, The viscosity of a concentrated suspension of spherical particles, J Colloid Sci 6 (1951)162-170.
- [46] JG. Brodnyan, The concentration dependence of the Newtonian viscosity of prolate ellipsoids, Trans Soc Rheol 3 (1959) 61-68.
- [47] U.J. Counto, Effect of the elastic modulus, creep and creep recovery of concrete, Mag Concr Res 16 (1964) 129-138.
- [48] V. Cannillo, F. Bondioli, L. Lusvarghi, M. Montorsi, M. Avella, M. Errico, and M. Malinconico, Modeling of ceramic particles filled polymer–matrix nanocomposites, Compos Sci Technol 66 (2006) 1030-1037.
- [49] H. Liu, and L. Brinson L, Mimicking mussel adhesion to improve interfacial properties in composites, Compos Sci Technol 68 (2008)1502.
- [50] H. Vo, M. Todd, G. Shi, A. Shapiro, M. Edwards, Towards model-based engineering of underfill materials: CTE modeling, Microelectron J. 32 (2001) 331.

- [51] D. Brown, V. Marcadon, P. Mele, N. Alberola, Effect of particle size on the properties of model nanocomposites, *Macromolecules* 41 (2008) 1499.
- [52] G. Voros, B. Pukanszky, Stress distribution in particulate filled composites and its effect on micromechanical deformation, *J Mater Sci*, 30 (1995) 4171.
- [53] G. Voros, B. Pukanszky, Effect of a soft interlayer with changing properties on the stress distribution around inclusions and yielding of composites, *Compos Part A: Appl Sci Manuf* 32 (2001) 343-352.
- [54] Z. Dominkovics, J. Hari, J. Kovacs, E. Fekete, B. Pukanszky, Estimation of interphase thickness and properties in PP/layered silicate nanocomposites, *Euro Polym J*, 47(2011) 1765-1774.
- [55] R. Qiao, L. Brinson, Simulation of interphase percolation and gradients in polymer nanocomposites, *Compos Sci Technol* 69(2009) 491.
- [56] S. Boutaleb, F. Zairi, A. Mesbah, M. Nait-Abdelaziz, J. Gloaquen, T. Boukharouba, J. Lefebvre, Micromechanics-based modeling of stiffness and yield stress for silica/polymer nanocomposites, *Intl J Solids Struct* 46 (2009) 1716.
- [57] Y. Dong, D. Bhattacharyya, A simple micromechanical approach to predict mechanical behavior of polypropylene/organoclay nanocomposites based on representative volume element (RVE), *Comput Mater Sci* 49 (2010) 1.
- [58] Y. Li, A. Waas, E. Arruda, A closed form, hierarchical, multi-interphase model for composites: derivation, verification and application to nanocomposites, *J. Mech Phys Solids* 59 (2011) 43.

- [59] H. Zhang, Z. Zhang, K. Friedrich, C. Eger, Property improvements on in situ epoxy nanocomposites with reduced interparticle distance at high nanosilica content, *Acta Mater* 54 (2006) 1833.
- [60] A. Muller, J-S. Jang, J. Suhr, RF. Gibson, Influence of particle diameter on coefficient of thermal expansion of SiO<sub>2</sub>/epoxy particulate composites, *Proc SAMPE Fall Tech. Conf.*, Salt Lake City, UT (2010).